5-23-2013

Plasmonic tuning of silver nanowires by laser shock induced lateral compression

Prashant Kumar
Birck Nanotechnology Center, Purdue University, kumar131@purdue.edu

Ji Li
Birck Nanotechnology Center, Purdue University

Qiong Nian
Birck Nanotechnology Center, Purdue University, qnian@purdue.edu

Yaowu Hu
Birck Nanotechnology Center, Purdue University, hu225@purdue.edu

Gary J. Cheng
Birck Nanotechnology Center, Purdue University, gjcheng@purdue.edu

Nanoscale

RSC Publishing

COMMUNICATION

View Article Online
View Journal | View Issue

Plasmonic tuning of silver nanowires by laser shock induced lateral compression

Cite this: *Nanoscale*, 2013, **5**, 6311

Prashant Kumar,†[ab] Ji Li,†[ab] Qiong Nian,[ab] Yaowu Hu[ab] and Gary J. Cheng*[abc]

Received 26th April 2013
Accepted 23rd May 2013

DOI: 10.1039/c3nr02104a

www.rsc.org/nanoscale

Laser shock induced lateral compression has been demonstrated to controllably flatten cylindrical silver nanowires. Nanowires with circular cross-sections of diameter 70 nm are significantly shaped laterally, which transformed them to metallic ribbons of huge width of 290 nm and of thickness down to 13 nm, amounting the aspect ratio to as high as 22, at a laser intensity of 0.30 GW cm^{-2}. Above the laser intensity of 0.30 GW cm^{-2} though, nanowires are observed to be ruptured. Lateral deformations of nanowires are achieved without altering longitudinal dimensions. Selected area electron diffraction patterns on the laterally deformed nanowires reveal that the flattening gives rise to twinning under high strain rate deformation without actually degrading crystallinity. As the 1D nanowire turns into a 2D metallic nanoribbon, new plasmonic modes and their combinations emerge. The transverse plasmon mode does not shift substantially, whereas longitudinal modes and their combinations are greatly influenced by lateral deformation. Apart from the transverse mode, which is dominant in a 1D nanowire and diminishes heavily when lateral deformation occurs, there is a presence of several longitudinal plasmonic modes and their combinations for metallic nanoribbons, which are revealed by experimental extinction spectra and also supported by finite-difference time-domain (FDTD) simulation. Such plasmonic tuning of silver nanowires across the visible range demonstrates the capability of a laser shock induced lateral compression technique for various emerging plasmonic applications. The laser shock compression technique has the advantages of flexibility, selectivity and tunability while retaining crystallinity of metallic nanowires, all of which enable it to be a potential candidate for plasmonic tuning of nanogeometries.

Introduction

When noble metals interact with light, they exhibit an interesting behavior of their electrons collectively oscillating. Such collective oscillatory behavior of electrons, called plasmons, depends on factors such as the geometry, dimensions of metallic nanostructures, the availability of conduction electrons in the concerned metal, dielectric function of a metallic nanostructure, and dielectric function of the medium it is surrounded with. Light couples with geometries made up of noble metals, in a more pronounced manner, when at least one of its dimensions is below 100 nm. There has been growing interest in plasmonics due to its potential promising applications.[1–6] Plasmonic modes can precisely be controlled by controlling the particle shape, size and size distribution.[2,7–10] From plasmonics perspective, nanowires are very special due to their anisotropic shape. For example, silver nanowires have been extensively studied for their plasmonic behavior.[11–18] Diameter dependence of plasmons has earlier been investigated for silver nanowires.[19,20] Non-circular cross-sections of nanowires exhibit interesting plasmonic modes due to inherent anisotropy.[21] Eccentricity dependence of plasmonic modes for ellipsoidal cross-section nanowires has earlier been studied.[22] Most of the presently existing literature on plasmonic dependence on the shape and size of nanowires are synthesized from bottom up approaches. In most of the cases, with the diameter variation of nanowires under study, crystallinity too varies which makes it difficult to distinguish the effects of dimension and crystallinity of nanowires on their plasmonic behavior. Moreover, synthesizing flat metallic ribbons with few nm thicknesses in a controllable manner is a big challenge. Laser shock induced lateral compression (LSILC) is an innovative *top-down* approach to achieve flattening of metallic nanowires with high precision, without compromising on crystalline quality.[23] This technique can be used to achieve the desired width of metallic ribbons, starting from the original nanowires having circular cross-sections.

Here in this article, we report on the effect of flattening of silver nanowires by LSILC on its plasmonic behaviour. Field emission scanning electron microscopy of cross-sections and transmission electron microscopy were employed for the quantification of the aspect ratio of flattened nanowires by LSILC. Selected area electron diffraction was utilized for

[a]*Birck Nanotechnology Center, Purdue University, West Lafayette, IN 47906, USA. E-mail: gjcheng@purdue.edu; Tel: +1-765-49-45436*
[b]*School of Industrial Engineering, Purdue University, West Lafayette, IN 47906, USA*
[c]*School of Mechanical Engineering, Purdue University, West Lafayette, IN 47906, USA*
† Authors made equal contribution to the paper.

crystallinity diagnosis. UV-VIS-NIR transmission spectroscopy was used to investigate the effect of flattening on plasmonic behaviour. Finite-difference time-domain (FDTD) simulation was carried out to validate experimental findings.

Experimental methods

Silver nanowires of diameter 60–70 nm and of length 7 μm (Blue Nano, NC, USA) were flattened employing laser shock compression, using short pulsed (5 ns) Q-switch Nd-YAG laser (Continuum Surelite III), details of which were reported elsewhere.[23] In brief, confinement media (clinical glass slides) and sacrificial layer 5 μm coating of aerosol graphite painting (Asbury Carbons, U.S.A.) on a 4 μm thin Al foil (Lebow Company Inc., Bellevue, WA) are used in sequence in the laser path, before it is incident on silver nanowires as shown in Fig. 1(a). Silver nanowires were dip coated (MTI Corporation, model no. EQHWTL-01-A) at a coating speed of 40 mm min^{-1} on a 4 μm thick free-standing aluminum foil using ethanol as the dispersing medium, and for dispersion of nanowires; an ultrasonicator (VWR-B1500A-DTH) was employed. For a cushion layer, PVA (Sigma-Aldrich) was dip coated on the back side of the Al foil. The whole assembly was fixed to a motorized X–Y stage. In this manner, we achieve high laser intensity (in the range of GW cm^{-2}) which exerts pressure on silver nanowires, as the heat generated due to laser is being consumed by an ablative sacrificial layer to pass on the pressure to the nanowire samples. Beam area was controlled using a focusing lens and the beam diameter used in the present experiment was 4 mm. Laser power was monitored by a power meter (Newport, type: 1916c). A focused ion beam (FEI Nova 200 Nano-Lab DualBeam TMSEM/FIB) was used for cutting nanowires and hence attaining cross-sections. A FESEM (Hitachi S-4800 field-emission scanning electron microscope) was used to image the cross-section. A transmission electron microscope (FEI Tecnai) was used for achieving microscopy as well as for acquiring a selected area electron diffraction pattern. UV-VIS-NIR transmission spectroscopy was carried out with a spectrometer (Perkin Elmer, model no. Lambda 950) for the wavelength range 200–1000 nm. A finite-difference time-domain (FDTD) simulation technique (Lumerical Solutions, Inc.) has been employed for plasmonic modeling for a few geometries to validate experimental findings.

Results and discussion

Silver nanowires that have undergone LSILC yield nanowires with thickness reduced and width broadened as can clearly be seen from cross-sectional images shown in Fig. 1(b). Silver nanowires, which originally had circular cross-sections, are heavily compressed due to laser shock induced pressure and their cross-sections turned out to be flattened. We do not observe any longitudinal deformation of nanowires in the present case and the only deformation present is the lateral compression. As laser parameters such as pulse width, confining media, and sacrificial layers were the same for all the experiments carried out by us, the effective laser shock induced pressure would be determined by laser intensity. Above 0.14 GW cm^{-2} laser intensity which gives rise to an equivalent laser pressure of 500 MPa, which is one order of magnitude higher than the yield strength for a silver material, plastic compression commences. In the laser intensity range of 0.14–0.30 GW cm^{-2}, *i.e.* in the effective laser pressure of 500–750 MPa, compressive strain increases with the increase in laser pressure. Above 0.30 GW cm^{-2}, which is equivalent to an effective laser pressure of 750 MPa, the nanowires get crushed. Silver nanowires exhibit very good ductility towards lateral compression, as has been observed in this experiment. Our experiment involves high strain rate ($\sim 10^7$ s^{-1}) deformation. Due to the high strain rate, silver nanowires exhibit superplasticity during the compression.

The microstructure changes achieved due to laser shock compression of nanowires were imaged by transmission electron microscopy, as shown in Fig. 2. With the increase of laser intensity, width of the resulting silver ribbons increases monotonically and the thickness is curtailed. Volume of nanowires remains constant in the process and the circular cross-section (diameter D) turns to a shape that is close to a rectangular one (dimensions W and h). Therefore, $(\text{area}_1)L = (\text{area}_2)L$ which means $(\pi D^2/4) = Wt$ and therefore, $t = \pi D^2/4W$ which

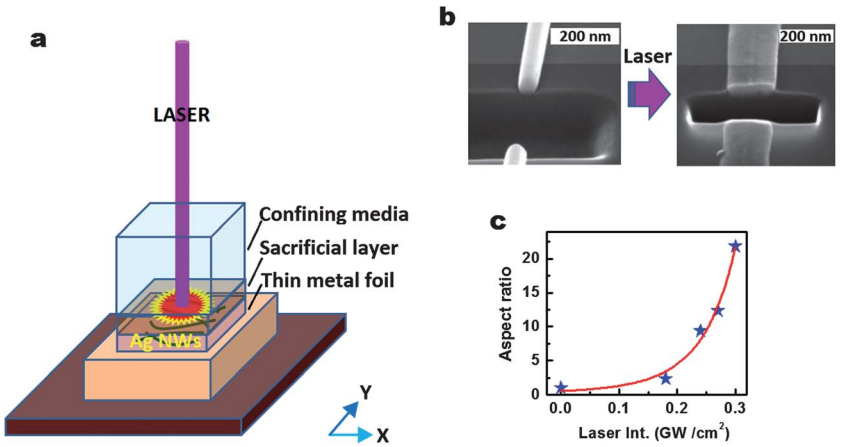

Fig. 1 (a) Schematic diagram for laser shock induced compression of silver nanowires, (b) FESEM image of silver nanowire cross-sections before and after laser induced compression achieved at 0.24 GW cm^{-2}. (c) Aspect ratio *vs.* laser intensity plot.

gives the aspect ratio a = width (W)/thickness (t) = $4\,W^2/\pi D^2 = 1.274W^2/D^2$. As can be seen in Fig. 2(a), the original non-deformed silver nanowires with circular cross-sections have the approximate diameter of ~70 nm. Fig. 2(b)–(e) show TEM images for flattened nanowires achieved *via* the LSILC technique. At the maximum laser intensity of 0.30 GW cm^{-2}, the width increases to 290 nm and the thickness reduces to 13 nm which amounts to a huge aspect ratio (width/thickness) of approximately 22. The laser intensity dependence on the resultant aspect ratio of nanowires is shown in Fig. 1(c). Fig. 2(f)–(j) show selected area electron diffraction (SAED) patterns for the TEM images shown in Fig. 2(a)–(e) respectively. The silver nanowires were originally highly crystalline and defect free. While SAED patterns in Fig 2(f) and (g) correspond to zone axes [001] and [011] respectively, the pattern shown in Fig. 2(h) corresponds to the combination of [112] and [001]. Similarly Fig. 2(i) and (j) correspond to the combination of zone axes [001] and [011]; [011] and [111] respectively. Fig. 2(k) shows twinned features in HRTEM. Fig. 2(l) is a zoomed image for a selected area in Fig. 2(k). We observe that the twinned feature corresponds to two sets of planes namely [200] and [11$\bar{1}$]. Fig. 2(m) shows dislocation clusters.

The presence of twins in laterally compressed nanowires showcases the deformability of nanowires. The present technique, however, does not degrade crystallinity, but rather maintains the FCC structure. Dislocation density in the plastically deformed NWs is observed to be relatively low as compared to that of its bulk counterpart. The principal deformation mechanism for silver nanowires while LSILC occurs is governed by the formation of twinned features and stacking faults. Nanowires having smaller cross-sections would be heavily twinned as compared to those with larger cross-sections. Apart from the cross-section, a ultrahigh strain rate in the range of 10^7 s^{-1} in the present experiment is responsible for the formation of twinning. Availability of longitudinal dimensions for movement of dislocations gives rise to dislocation clusters. However, the density of

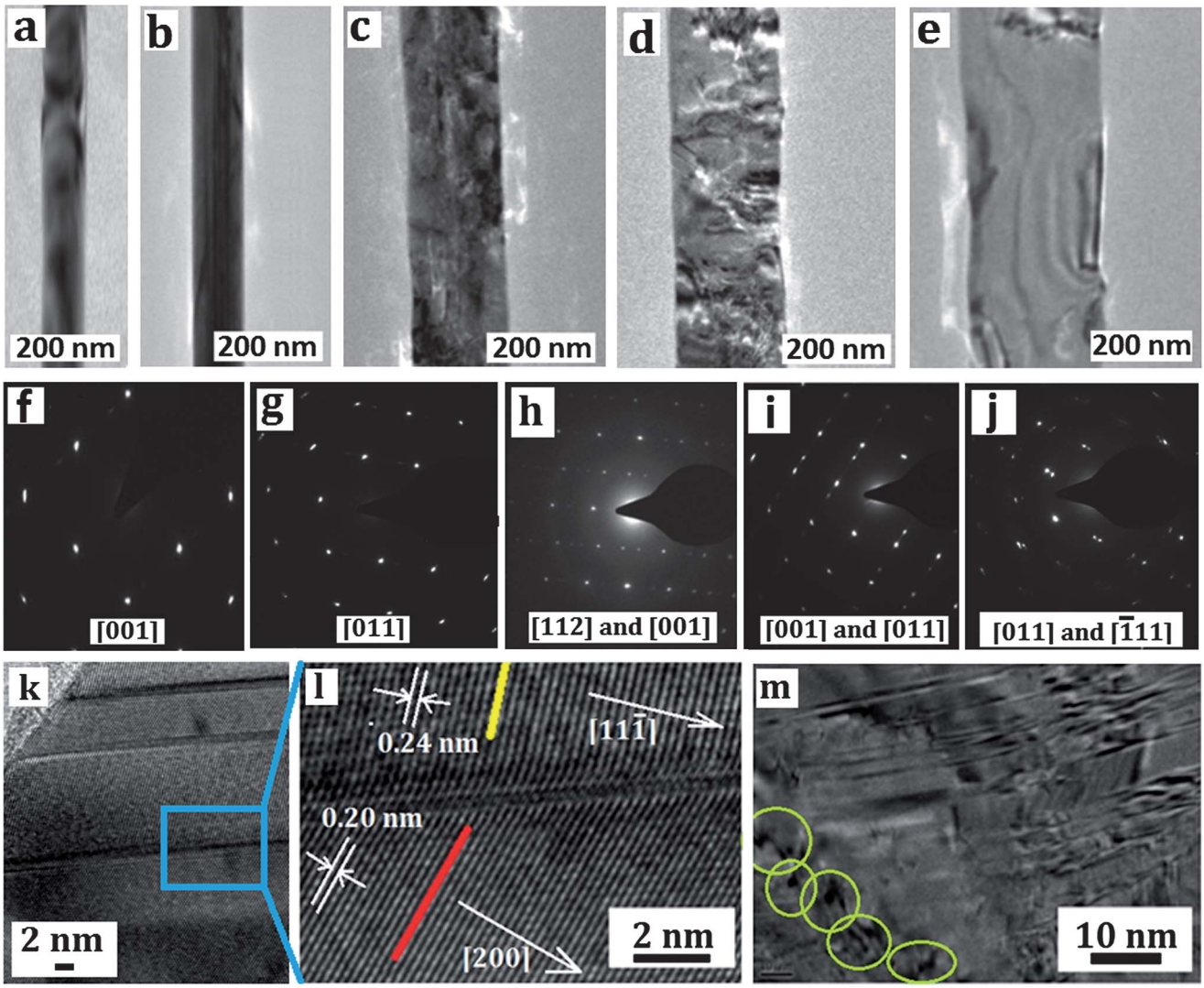

Fig. 2 TEM images for a silver nanowire (a) before any treatment and after laser shock compression at (b) 0.18, (c) 0.24, (d) 0.27 and (e) 0.30 GW cm^{-2}. Selected area electron diffraction (SAED) pattern corresponding to (a)–(e) is shown in (f)–(j). Twinning features formed and dislocation clusters are shown in high resolution images in (k) and (l) respectively.

such dislocation clusters is quite marginal in most of the cases except for severely deformed or ruptured ribbons. Such tunability from circular cross-section nanowires to the thin silver ribbons demonstrates the tremendous capability of the LSILC technique. Importantly, huge flattening yet maintaining the crystalline building blocks is a great achievement by this emerging technique of laser shock compression. This technique can invariably be employed to transform any nanowires with circular cross-sections to ribbons, if the material is ductile. Such a technique can even be generalized for other nanogeometries.

Having achieved a great degree of morphological control for silver nanowires, as evidenced by the maximum achieved aspect ratio of 22, we were poised to investigate optical behaviour of such laser shock shaped nanowires, as optical properties of plasmonic materials are dimension sensitive. To our surprise, we indeed got a very strong effect of laser shaping on the plasmonic behaviour. Fig. 3(a) shows extinction spectra for nanowires compressed at different laser intensity values till 0.30 GWcm^{-2}. 1D nanowires show a predominant transverse plasmonic peak with a marginal longitudinal peak. However, as the extent of lateral compression is gradually raised, the longitudinal peak gets stronger and suppresses the transverse plasmonic mode. Remarkably, as the LSILC process laterally deforms silver nanowires, new longitudinal plasmonic modes emerge and their combinations are also observed. The trend of wavelength maxima in extinction spectra *vs.* the aspect ratio is shown in Fig. 3(b) for different plasmonic modes. It is observed that the transverse mode does not shift much, while longitudinal modes are very sensitive to lateral deformations. The tunable plasmon peak across the visible range demonstrates that LSILC can indeed be utilized for plasmonic tuning of nanowires.

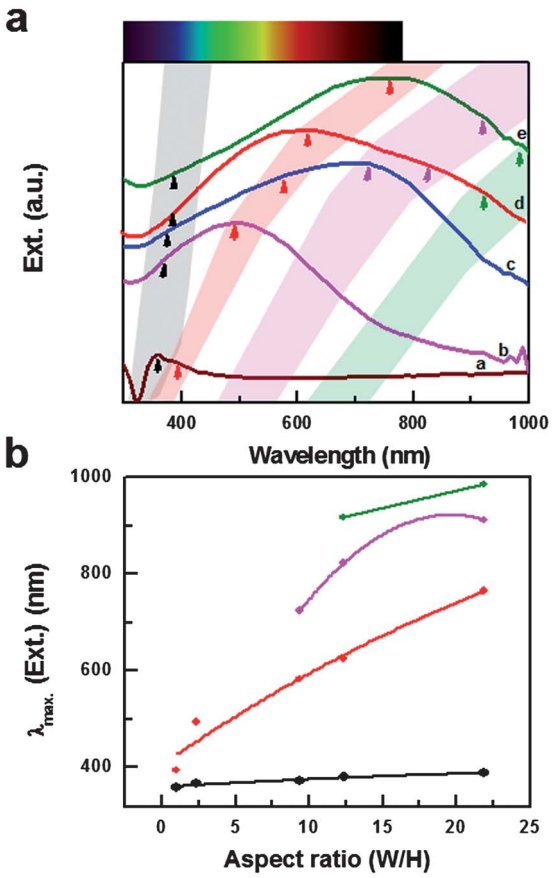

Fig. 3 (a) UV-VIS-NIR extinction spectra for a silver nanowire: a. before any treatment and after laser shock compression at b. 0.18, c. 0.24, d. 0.27 and d. 0.30 GW cm^{-2}. (b) Trends of wavelength maxima for extinction spectra.

Plasmons do originate due to the conduction electrons in plasmonic materials and is strongly dependent upon the dielectric surrounding it. Since the number of available conduction electrons would be determined by the dimension of nanomaterials, plasmonic frequency would be dependent on dimensions. The mechanism of absorption of light by plasmonic metal particles was suggested by Gustav Mie, based on the solution of Maxwell's equations.[24] When an electromagnetic field interacts with the plasmonic particle, local charge separation takes place. Absorption of light has been demonstrated to be shape and size dependent and also dependent on environment.[25] For tiny spherical particles with volume V_0 having a dielectric constant

$$\varepsilon(\lambda) = \varepsilon_1(\lambda) + i\varepsilon_2(\lambda) \quad (1)$$

dispersed in an isotropic non-absorbing medium having a dielectric constant ε_m, Mie's theory gives the extinction cross-section:

$$\sigma_{ext}(\lambda) = (18\pi/\lambda)\varepsilon_m^{3/2} V_0 \{\varepsilon_2(\lambda)/(\varepsilon_1(\lambda) + 2\varepsilon_m^2) + \varepsilon_2(\lambda)^2\} \quad (2)$$

where, λ is the wavelength of the incident light and c is the velocity of light. The above equation holds true for tiny particles dispersed in isotropic media and does not give any clue for the absorption peak for other nanogeometries and for size dependence. The extinction cross-section for elongated ellipsoids can be derived by Gan's treatment:[26]

$$\sigma_{ext}(\lambda) = (2\pi/3\lambda)\varepsilon_m^{3/2} V \sum \{(1/P_j^2)\varepsilon_2(\lambda)\}/\{\varepsilon_1(\lambda) + (1 - P_j)/P_j\varepsilon_m^2 + \varepsilon_2(\lambda)^2\} \quad (3)$$

where P_x, P_y and P_z are the depolarization factors along the three axes namely X, Y and Z respectively which seek to restore the original electronic configurations. Now, for the ellipsoidal nanorod with

$$X > Y = Z \text{ and aspect ratio } R = Y/X$$

$$P_X = (1 - e^2)/e^2[1/2e\ln\{(1 + e)/(1 - e)\} - 1] \quad (4)$$

$$P_Y = P_Z = (1 - P_X)/2$$

where,

$$e = (1 - (Y/X)^2) = (1 - 1/R^2)^{1/2}$$

Gan's treatment suggests transverse and longitudinal modes for ellipsoidal nanorods which can even hold fairly good for

nanowires of circular cross-sections as it satisfies $X > Y = Z$. The theory reveals that while the transverse mode is unaffected by aspect ratio, the longitudinal mode is heavily dependent on it. The longitudinal plasmonic peak usually gets red-shifted with the enhancement of the length/diameter ratio. On the other hand, the absorption peak corresponding to the transverse mode does not alter.[27,28] The present case under our investigation is completely different where a nanowire of a circular cross-section is being flattened into a rectangular cross-section. Such flattened ribbons would give rise to variation in electrostatic charges along their widths too, which would give rise to another plasmonic mode, as compared to that for the thinner nanowires of circular cross-sections. In addition, plasmon modes along the length and the width would interfere with each other.

Schematic diagrams of two kinds of plasmonic modes, namely transverse and longitudinal modes, which are feasible in cylindrical nanowires, are shown in Fig. 4a and b respectively. One can have either dipole or multipole in the transverse mode itself, depending on how the light couples with the nanowires. Interaction of light with metallic nanowires and consequent electronic oscillation amplitude and directions can conveniently be thought to be equivalent to the situation where metallic surfaces have electronic charges and associated electric field distributions. As the nanowires with circular cross-sections turn to that with rectangular cross-sections (or into ribbons), several plasmonic modes can appear (see Fig. 4c–f). There would always be a possibility of coexistence of two or more of such plasmonic modes for ribbons of large widths. Thus, when light is incident upon nanowires with circular cross-sections (original nanowires), less number of modes are feasible. Whereas, on the other hand, in the case of ribbons achieved by laser shock compression, several longitudinal and transverse plasmonic modes and their hybrids can coexist. Existence of longitudinal and transverse plasmon modes in plasmonic material nanowires has earlier been used for its coupling to the plasmon of nanospheres.[29] Multipole plasmons have also been observed.[30,31] Usually, nanowires of smaller diameters are expected to support higher orders of transverse modes and their hybrids. Liu and Willis[32] have demonstrated that when thickness of thin monolayers of silver is increased, 2D sheet plasmons would convert into 3D plasmons. Thus plasmonic behaviour is governed by thickness of the 2D sheet. As the width of a nanoribbon is gradually enhanced and thickness is curtailed in the process of laser shock compression, aspect ratio = width/thickness keeps on increasing keeping the length intact. Such a transformation of shapes would have effects similar to the length increase and diameter decrease of a nanowire. However, the two effects would not be the same; red-shift of the plasmon peak and bandwidth would also depend on how the plasmonic modes hybrid themselves in plane. Our experimental report is the first of its kind towards understanding plasmons for such shape transitions from nanowires to ribbons achieved *via* LSILC.

FDTD results for spatial charge density distribution in Fig. 5 show transverse modes (b, d, and g) and the combinatorial plasmonic modes (e and h) corresponding to the two directions normal to each other for original nanowires as well as for the LSILC deformed AgNWs. These simulated plasmonic modes seem to be consistent with the modes as indicated in the extinction peaks in Fig. 3(a). It could be seen from Fig. 3(a) that there are primarily one transverse mode (shown by black arrows) and at least one of the longitudinal modes (shown by red, pink and green arrows) present in the LSILC treated AgNWs. It should be noted that these peaks would not remain unaltered as they would interfere and would thus influence each other. Therefore, these peaks are usually observed to be shifted. We have achieved multiple plasmonic modes in Ag nanoribbons.

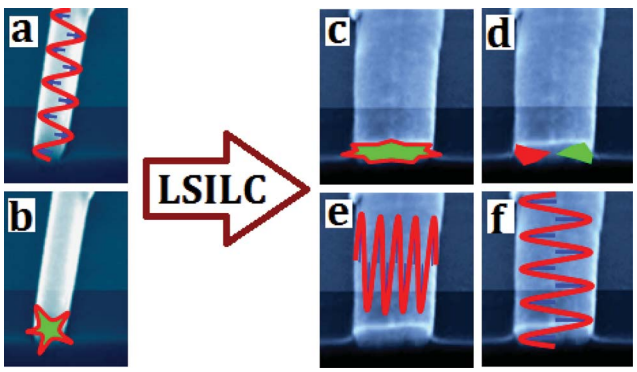

Fig. 4 Possible plasmonic modes in silver nanowires with circular cross-sections before LSILC (as shown in (a) and (b)) and after LSILC when the cross-sections turn rectangular (shown in (c)–(f)).

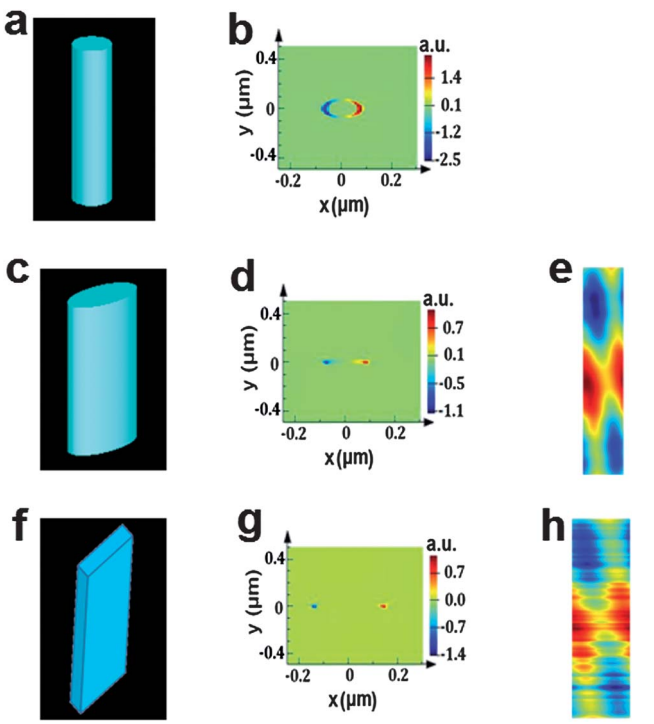

Fig. 5 FDTD simulation results for spatial charge density distribution for transverse modes (b, d, and g) and resultant interfering longitudinal modes (e, h) for cylindrical Ag nanowires with circular cross-sections ($R = 70$ nm, $L = 12$ μm) (top panel), cylindrical Ag nanowires with oval cross-sections ($R_1 = 95$ nm, $R_2 = 10$ nm, $L = 12$ μm) (middle panel) and rectangular Ag nanoribbon ($L = 12$, $W = 290$ nm, $t = 13$ nm) (bottom panel). A plane wave source was considered for the purpose and the distributions are for a source with a fixed wavelength of 500 nm.

In general, for a single plasmon band, the peak width has to do with the dephasing of the coherent electron oscillation.[33,34] According to the Fermi liquid theory,[35] the rate of scattering among electrons would be directly proportional to the square of the difference of the excited state energy and the Fermi energy E_F. The phase relaxation, electron–electron scattering and electron–phonon energy relaxation occur on the order of 10 fs, 100 fs and 1 ps, respectively.

Thus, the contribution of electron–electron scattering would be more pronounced than that due to electron–phonon interactions. Larger plasmon peak widths usually would correspond to a rapid loss of the coherence. For uniform size distribution and hence homogeneous line broadening, the total dephasing time can therefore be calculated from the plasmon peak width. For example, it has been reported that spherical 20 nm gold nanoparticles would have a dephasing time of 4.1 fs and for 100 nm diameter particles though, it would be only 2.6 fs.[33] Thus, the larger the diameter, the faster is the dephasing and the broader would be the plasmon peak. For the present study, though, the extinction spectra for a particular ribbon would comprise all possible modes, and the mode which dominates would give rise to global maxima in extinction spectra. However, broadening would occur due to the size effect and also due to defects generated therein even though it may be pretty small in volume fraction and would indirectly affect the relaxation. Shoulder-like features, on the other hand, do exist due to the availability of multiple modes.

In conclusion, flattening of silver nanowires of circular cross-sections achieved by laser shock pressure as evidenced by the aspect ratio as high as 22 for the silver ribbons is encouraging. There is a comfortable working window of laser intensity 0.14–0.30 GW cm^{-2} for the lateral compression of silver nanowires. It is gratifying to note that flattening achieved *via* LSILC does not degrade crystallinity and the nanowires hold on their FCC structure. It is noteworthy that such drastic lateral compression of nanowires has an immense impact on the plasmon bands. Transverse modes are not effectively influenced (feeble effect though) by LSILC processing, while longitudinal modes are sensitive to such processing. New plasmonic bands have been observed which were not present in original nanowires, which possibly arise due to the newly found access along the width. In addition, various plasmonic modes influence each other. Last but not the least, metallic nanoribbons achieved *via* the present technique described in this article are unique in many senses, as they have been achieved by a (a) single-step, (b) clean and (c) optical processing technique and are expected to have several potential applications including that as electrodes in FET devices, as SERS materials and in plasmonic wave guiding. Such tunability of plasmonic peaks with LSILC seems destined for their use in controllable plasmonic tuning of other ductile plasmonic nanomaterials and hence broadening the scope of this emergent technique.

Acknowledgements

The authors want to thank the financial support from NSF CAREER Award (CMMI-0547636), NSF Grant (CMMI 0928752) through the program of Materials Processing & Manufacturing, and Purdue Research Foundation research incentive award.

References

1 W. L. Barnes, A. Dereux and T. W. Ebbesen, *Nature*, 2003, **424**, 824.
2 J. A. Scholl, A. L. Koh and J. A. Dionne, *Nature*, 2012, **483**, 421.
3 S. Lal, S. Link and N. J. Halas, *Nat. Photonics*, 2007, **1**, 641.
4 R. Yan, P. Pausauskie, J. Huang and P. Yang, *Proc. Natl. Acad. Sci. U. S. A.*, 2009, **106**, 21045.
5 M. I. Stockman, *Opt. Express*, 2011, **19**, 22029.
6 S. Hayashi and T. Okamoto, *J. Phys. D: Appl. Phys.*, 2012, **45**, 433001.
7 Y. Lin, X. Q. Liu, T. Wang, C. Chen, H. Wu, L. Liao and C. Liu, *Nanotechnology*, 2013, **24**, 125705.
8 P. Kumar and M. G. Krishna, *Phys. Status Solidi A*, 2010, **207**, 947.
9 S. J. Tan, M. J. Campolongo, D. Luo and W. Cheng, *Nat. Nanotechnol.*, 2011, **6**, 268.
10 S. Link and Mostafa. A. El-Sayed, *Int. Rev. Phys. Chem.*, 2000, **19**, 409.
11 H. Wei, S. Zhang, X. Tian and H. Xu, *Proc. Natl. Acad. Sci. U. S. A.*, 2013, **110**, 4494–4499.
12 A. L. Pyayt, B. Wiley, Y. Xia, A. Chen and L. Dalton, *Nat. Nanotechnol.*, 2008, **3**, 660.
13 Z. Li, F. Hao, Y. Huang, Y. Fang, P. Nordlander and H. Xu, *Nano Lett.*, 2009, **9**, 4383.
14 H. Ditlbacher, A. Hohenau, D. Wagner, U. Kreibig, M. Rogers, F. Hofer, F. R. Aussenegg and J. R. Krenn, *Phys. Rev. Lett.*, 2005, **95**, 257403.
15 Y. Sun, B. Gates, B. Mayers and Y. Xia, *Nano Lett.*, 2002, **2**, 165.
16 M. N'Gom, J. Ringnalda, J. F. Mansfield, A. Agarwal, N. Kotov, N. J. Zaluzec and T. B. Norris, *Nano Lett.*, 2008, **8**, 3200.
17 Z. Li, S. Zhang, N. J. Halas, P. Nordlander and H. Xu, *Small*, 2011, **7**, 593.
18 H. Ditlbacher, A. Hohenau, D. Wagner, U. Kreibig, M. Rogers, F. Hofer, F. R. Aussenegg and J. R. Krenn, *Phys. Rev. Lett.*, 2005, **95**, 257403.
19 M. S Stewart, C. Qiu, R. Kattumenu, S. Singamaneni and C. Jiang, *Nanotechnology*, 2011, **22**, 275712.
20 C. J. Murphy and N. R. Jana, *Adv. Mater.*, 2002, **14**, 80.
21 J. P. Kottmann, O. J. F. Martin, D. R. Smith and S. Schultz, *Phys. Rev. B: Condens. Matter Mater. Phys.*, 2001, **64**, 235402.
22 J. M. Oliva and S. K. Gray, *Chem. Phys. Lett.*, 2006, **427**, 383.
23 J. Li, Y. Liao, S. Suslov and G. J. Cheng, *Nano Lett.*, 2012, **12**, 3224.
24 G. Mie, *Ann. Phys.*, 1908, **330**, 377.
25 L. M. Liz-Marzan, M. A. Correa-Duarte, I. Pastoriza-Santos, P. Mulvaney, T. Ung, M. Giersig, N. A. Kotov, *Handbook of surfaces and interfaces of materials: core-shell nanoparticles and assemblies thereof*, Academic Press, San Diego, 2001, vol. 3, ch. 5.
26 R. Gans, *Ann. Phys.*, 1915, **47**, 270.

27 Y. Yu, S. Chang, C. Lee and C. R. C. Wang, *J. Phys. Chem. B*, 1997, **101**, 6661.
28 S. Link, M. B. Mohamed and M. A. El-Sayed, *J. Phys. Chem. B*, 1999, **103**, 3073.
29 S. Kim, K. Imura, M. Lee, T. Narushima, H. Okamoto and D. H. Jeong, *Phys. Chem. Chem. Phys.*, 2013, **15**, 4146.
30 E. K. Payne, K. L. Shuford, S. Park, G. C. Schatz and C. A. Mirkin, Multipole plasmon resonances in gold nanorods, *J. Phys. Chem. B*, 2006, **110**, 2150.
31 L. S. Slaughter, W.-S. Chang, P. Swanglap, A. Tcherniak, B. P. Khanal, E. R. Zubarev and S. Link, *J. Phys. Chem. C*, 2010, **114**, 4934.
32 Y. Liu and R. F. Willis, *Surf. Sci.*, 2009, **603**, 2115.
33 S. Link and M. A. El-Sayed, *J. Phys. Chem. B*, 1999, **103**, 4212.
34 E. J. Heilweil and R. M. Hochstrasser, *J. Chem. Phys.*, 1985, **82**, 4762.
35 D. Pines and P. Nozieres, *The Theory of Quantum Liquids*, ed. W. A. Benjamin, New York, 1966.